A Hierarchical 3D TiO_2/Ni Nanostructure as an Efficient Hole-Extraction and Protection Layer for GaAs Photoanodes

Mahdi Alqahtani,*[a, b, c] Andreas Kafizas,[d, e] Sanjayan Sathasivam,[f] Mohamed Ebaid,[g] Fan Cui,[a] Ahmed Alyamani,[c] Hyeon-Ho Jeong,[h] Tung Chun Lee,[f, i] Peer Fischer,[h] Ivan Parkin,[f] Michael Grätzel,[j] and Jiang Wu*[a, b]

Photoelectrochemical (PEC) water splitting is a promising clean route to hydrogen fuel. The best-performing materials (III/V semiconductors) require surface passivation, as they are liable to corrosion, and a surface co-catalyst to facilitate water splitting. At present, optimal design combining photoelectrodes with oxygen evolution catalysts remains a significant materials challenge. Here, we demonstrate that nickel-coated amorphous three-dimensional (3D) TiO_2 core-shell nanorods on a TiO_2 thin film function as an efficient hole-extraction layer and serve as a protection layer for the GaAs photoanode. Transient-absorption spectroscopy (TAS) demonstrated the role of nickel-coated (3D) TiO_2 core-shell nanorods in prolonging photogenerated charge lifetimes in GaAs, resulting in a higher catalytic activity. This strategy may open the potential of utilizing this low-cost (3D) nanostructured catalyst for decorating narrow-band-gap semiconductor photoanodes for PEC water splitting devices.

[a] *Dr. M. Alqahtani, F. Cui, Prof. J. Wu*
Department of Electronic and Electrical Engineering
University College London
London WC1E 7JE (United Kingdom)
E-mail: mahdi.alqahtani.16@alumni.ucl.ac.uk
[b] *Dr. M. Alqahtani, Prof. J. Wu*
Institute of Fundamental and Frontier Sciences
University of Electronic Science and Technology of China
Chengdu 610054 (P. R. China)
E-mail: jiangwu@uestc.edu.cn
[c] *Dr. M. Alqahtani, Dr. A. Alyamani*
King Abdulaziz City for Science and Technology (KACST)
Riyadh 12371 (Saudi Arabia)
[d] *Dr. A. Kafizas*
Department of Chemistry
Imperial College London
London W12 0BZ (United Kingdom)
[e] *Dr. A. Kafizas*
The Grantham Institute
Imperial College London
London SW7 2AZ (United Kingdom)
[f] *Dr. S. Sathasivam, Dr. T. Chun Lee, Prof. I. Parkin*
Department of Chemistry
University College London
London WC1H 0AJ (United Kingdom)
[g] *Dr. M. Ebaid*
Joint Centre for Artificial Photosynthesis (JCAP)
Lawrence Berkeley National Laboratory
Berkeley, California 94720 (USA)
[h] *Dr. H.-H. Jeong, Prof. P. Fischer*
Max Planck Institute for Intelligent Systems
Heisenbergstraße 3, 70569 Stuttgart (Germany)
[i] *Dr. T. Chun Lee*
Institute for Materials Discovery
University College London
London WC1E 7JE (United Kingdom)
[j] *Prof. M. Grätzel*
Institute of Chemical Science and Engineering Faculty of Basic Science
Ecole Polytechnique Federale de Lausanne
1015 Lausanne (Switzerland)

Introduction

Energy consumption has increased rapidly in recent decades to meet the needs of a growing world population and economy.[1] Solar energy is our largest source of renewable energy and can easily meet all current energy demands.[2] In this context, photo-electrochemical (PEC) water splitting is a promising method to harvest solar energy and produce clean hydrogen fuel.[1,3] Although PEC cells have been intensively investigated for decades, a commercially viable technology is yet to be realized. Recent developments in single and multiband semiconductor (p-n junctions) have shown higher efficiencies by enhancing charge carrier separation and performance in PEC devices.[4] In addition, the formation of a p-n heterojunction can increase the photovoltage and enhance solar absorption.[5] On the other hand, The water oxidation reaction is considered the major bottleneck for the development of efficient photo-electrochemical devices, due to the slow kinetics of the transfer of four holes associated with water oxidation, a high oxygen evolution reaction (OER) overpotential is required.[6] Many semiconductors for PEC water splitting suffer from poor catalytic activity in driving the OER, and require surface co-catalysts improve the reaction kinetics.[7] Unfortunately, the most active co-catalysts for driving the OER reaction are composed of expensive and rare platinum group metals (e.g., Pt, RuO_2, and IrO_2). Moreover, their use is compounded by their optical properties, as they show strong absorption in the visible and therefore hamper light transmission into the photoactive semiconductor layer that lies beneath them.[8] In addition, the structure of catalyst can significantly impact PEC performance.[8] Finally, to achieve high efficiency PEC water splitting,[9] a narrow bandgap material is needed to absorb a significantly large portion of photons in the solar spectrum.

All the aforementioned requirements for a photoanode have not been realised in the most popularly studied materials, which include transition metal oxides, silicon and III–V semiconductors.[2a,10] The wide band gap and sluggish water oxidation kinetics of transition metal oxide photoanodes limits their solar-to-hydrogen (STH) conversion efficiency.[11] Silicon possesses a low open circuit voltage (typically 0.6 V), and therefore requires a high positive bias voltage (typically 1.1 V_{RHE}) to drive water oxidation.[12] However, III-V semiconductor materials, such as GaAs, exhibit high PEC performance and require less positive onset potentials for driving water oxidation (~0.5 V_{RHE}) owing to the excellent optical properties and suitable band potentials.[13] GaAs photoanodes are usually decorated with ultrathin catalyst and protection layers.[14] For example, metal overlayers, such as Pt grain, Au, Pd, and Ru have been deposited onto surface of GaAs photoelectrodes, but often showed low PEC performance due to the formation of electrically resistive Schottky barriers.[15]

Although it is understood that the thickness and structure of the protection layers and catalyst used must be precisely controlled to provide good electrical properties, for example, high hole mobility and their efficient extraction in the OER, the exact role played by surface protection layers remains unclear, and to date, has not been sufficiently addressed. To this end, we investigate GaAs photoanodes, and improve PEC performance by applying a three-dimensional (3D) TiO_2/Ni bi-functional nanostructure. The hierarchical TiO_2/Ni nanostructure includes a leaky amorphous TiO_2 layer thin film to isolate the GaAs surface from the solution and the 3D-TiO_2/Ni core-shell nanorods act as an effective means to transfer photo-excited holes from GaAs to the solution for water oxidation. Despite the fact that GaAs is not stable under anodic potential, One-dimensional photoelectrodes can significantly relax the requirement on the turnover frequency (TOF) of loaded electrocatalysts by reducing the photogenerated charge flux, and hence minimise recombination. This is particularly important in the case of electrochemical oxygen evolution reactions. However, nanowire photoelectrodes generally suffer from non-uniformity and their performance is limited by the worst-performing individual nanowire.[16] Therefore, the 3D/TiO_2/Ni core-shell nanostructure employed herein, on planar GaAs photoanodes, can alleviate the requirement for high performance electrocatalysis, while avoiding the fabrication challenges of uniform nanowire arrays. The hierarchical 3D/TiO_2/Ni nanostructure not only serves as a charge transfer channel to reduce the charge flux, but also avoids charge accumulation at the photoelectrode surface, and suppresses recombination of photocarriers at the semiconductor/electrolyte interface. Despite the fact that GaAs is more susceptible to photocorrosion under anodic potential than under cathodic potentials,[17] we introduce the hierarchical 3D/TiO_2/Ni bi-functional nanostructure, as both a charge transfer and a surface protection layer, to enhance the charge-separation efficiency and at the same time to reduce photocorrosion of the III-V photoanode.

Results and Discussion

TiO_2/Ni nanostructures on GaAs photoanodes

The surface co-catalyst structure, at both the nano and micro-scale, plays significant role in enhancing the PEC performance of photoanodes.[7a] Herein, n-type GaAs was employed as our photoanode for PEC water oxidation. To reduce the over-potential and improve PEC performance of III-V photoelectrodes in an electrolyte, hierarchical 3D-TiO_2/Ni nanostructures were fabricated on the GaAs surface as depicted in Figure 1. As shown in Figure 1a and d, an amorphous titanium dioxide (TiO_2) nanofilm (~6 nm) was first deposited onto the surface of n-GaAs photoanodes as a protection layer.[13,18] The amorphous TiO_2 nanorods and Ni co-catalysts were fabricated by glancing angle deposition (GLAD) to create a 3D hole extraction layer to facilitate the charge transfer to co-catalysts. Crucially, this GLAD method can independently control not only the size of TiO_2 nanorods by adjusting the amount of evaporants, but also the Ni coverage with an angle of the incident vapour flux towards nanorods (e.g., Figures 1c and f). The low magnification STEM image in Figure 1b shows that well-defined nanorods were formed on the surface of the GaAs substrate. High-resolution cross-sectional scanning transmission electron microscopy (STEM) images and energy-dispersive X-ray spectroscopy (EDX) mapping, as shown in Figure 1c, confirmed the formation of a 6 nm nanofilm underneath the nanorods and that the nanofilm and nanorods are amorphous. The high-resolution STEM images unambiguously show a sharp contrast between the TiO_2 nanofilm and GaAs epilayer, indicating good interface quality with marginal intermixing, and the EDX mapping confirms well coated Ni co-catalysts over entire TiO_2 nanorods, acting as a co-catalyst shell (see Supporting Information Figures S1–S8). To study the critical role of the hierarchical 3D-TiO_2/Ni nanostructures in promoting the OER, a sample was grown with Ni particles only deposited on the top of the TiO_2 nanorods, as shown in Figure 1d–f.

Photoelectrochemical performance of GaAs photoanodes

The GaAs photoanodes coated with the 3D TiO_2 nanostructures and Ni particles on the top of the 3D TiO_2, are referred to as "GaAs/TiO_2/Ni top nanorods". "The GaAs photoanodes coated with the 3D TiO_2 nanostructures and Ni particles on the top and sides of the 3D TiO_2, are referred to as "GaAs/TiO_2/Ni core-shell nanorods". A GaAs photoanode coated with only a TiO_2 nanofilm (i.e., no nanorods on top) is referred to as "GaAs/TiO_2 nanofilm". The PEC performance was measured using a standard three-electrode configuration, including a silver-silver chloride (Ag/AgCl) reference electrode, Pt coil counter electrode, and working electrode in 1.0 M NaOH electrolyte (pH = 14) under 1 sun illumination.

The photocurrent density-voltage (*J*–*V*) characteristics are shown in Figure 2a for the GaAs/TiO_2 nanofilm, GaAs/TiO_2/Ni top nanorods, and GaAs/TiO_2/Ni core-shell nanorods photoanodes. As shown from Figure 2a, the photocurrent of the

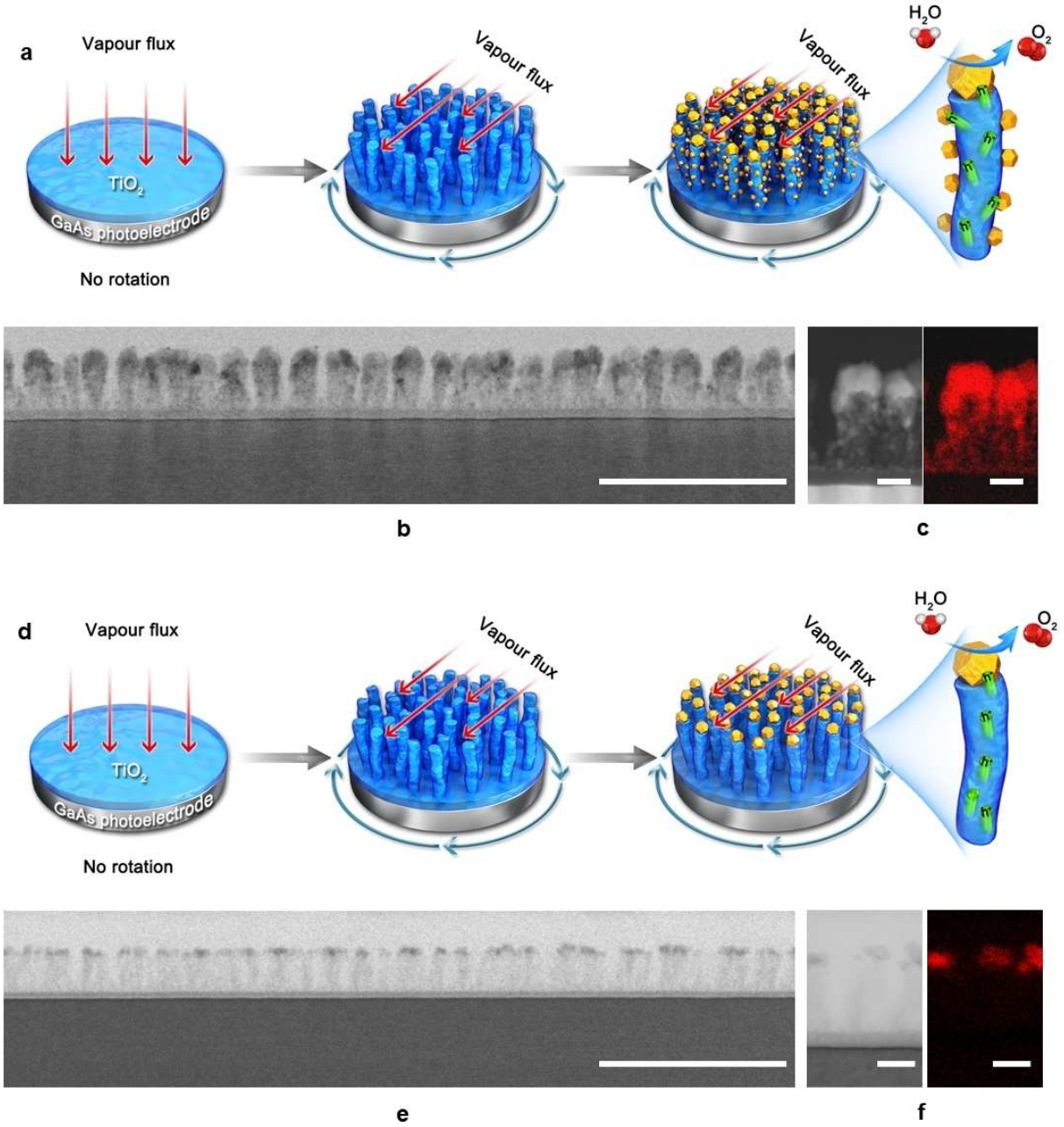

Figure 1. Surface modification and structural characterisation of hierarchical TiO_2/Ni nanostructure photoanodes. (a) Schematics of the growth of the hierarchical TiO_2/Ni nanostructure on a GaAs photoanode: growth of an amorphous TiO_2 nanofilm on GaAs with normal incident flux and no substrate rotation at ambient temperature, deposition of TiO_2 nanorods by GLAD, and coating Ni co-catalysts over the entire surface of the TiO_2 nanorods. (b) Cross-sectional TEM image of a hierarchical TiO_2/Ni nanostructure photoanode. The scale bar is 200 nm. (c) HAADF-STEM image of the photoanode surface structure and its corresponding STEM-EDX mapping, confirming the distribution of Ni. The scale bar is 20 nm. (d) Schematics of the growth of a reference photoanode with Ni co-catalyst only deposited on the top of the TiO_2 nanorods. (e) Cross-sectional TEM image of the photoanode illustrated in (d). The scale bar is 200 nm. (f) High-resolution TEM image of the photoanode surface structure and its corresponding EDX mapping, confirming that Ni co-catalyst was only found on the top of the TiO_2 nanorods. The scale bar is 20 nm.

GaAs/TiO_2 nanofilm photoanode reached ~8.43 mA cm^{-2} at 0 V vs Ag/AgCl (1.0 V vs RHE). By using the 3D TiO_2 hole-extraction layer deposited by the GLAD technique, a significant improvement in photocurrent was obtained; the photocurrent of the GaAs/TiO_2/Ni top nanorods was increased to around 10.42 mA cm^{-2} at 0 V vs Ag/AgCl, whereas the GaAs/TiO_2/Ni core-shell nanorods reached 12.87 mA cm^{-2} at the same bias voltage. The onset potentials for the GaAs/TiO_2 nanofilm, GaAs/TiO_2/Ni top nanorods, and GaAs/TiO_2/Ni core-shell nanorods photoanodes were −0.45, −0.53 and −0.68 V vs Ag/AgCl, respectively (0.58, 0.50, 0.35 V vs RHE, respectively). This shows that the 3D TiO_2 nanostructure has a marginal effect on reducing the onset potential (by ~0.08 V), but the addition of a Ni co-catalyst results in a more marked reduction (by ~0.15 V).

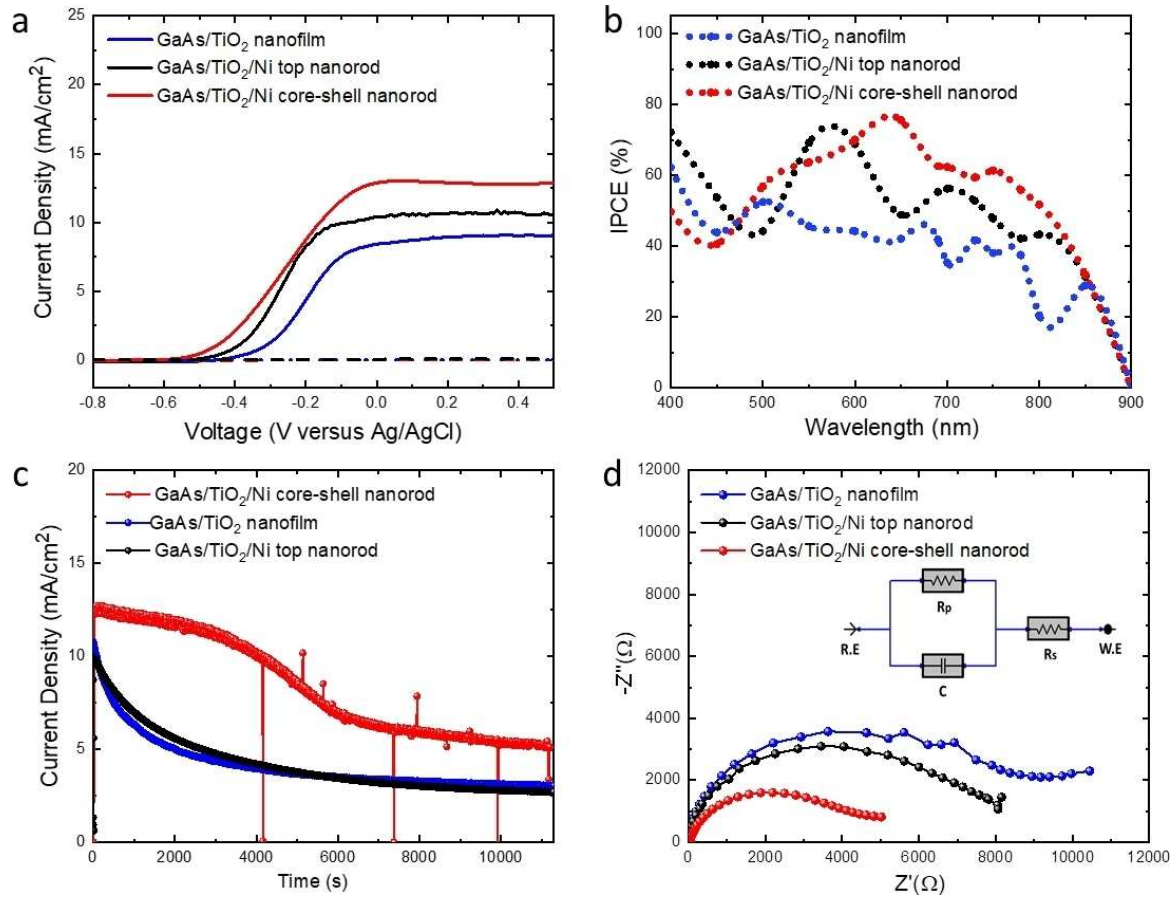

Figure 2. Photoelectrochemical measurements of GaAs photoanodes. (a) *J–V* curves (scan rate is 50 mV s^{-1}) in 1.0 M NaOH electrolyte (pH = 14) under 1 sun illumination versus reference electrode (Ag/AgCl). (b) IPCE of GaAs photoanodes at 0 V vs Ag/AgCl (1 V vs RHE). (c) *J–t* profile of both GaAs photoanodes at 0 V vs Ag/AgCl under simulated sunlight (AM1.5G filter, 100 mW cm^{-2}) for 3 h. (d) Nyquist plot under dark conditions for GaAs/TiO_2 nanofilm, GaAs/TiO_2/Ni core-shell nanorod, and GaAs/TiO_2/Ni top nanorod photoanodes with a perturbation amplitude 10 V and frequency range from 10 kHz to 3 MHz. The inset is the equivalent circuit model.

We attribute the improvement in photocurrent, and reduction in onset potential, to the enhancement in hole carrier transport to the electrolyte interface through the use of a 3D TiO_2 nanorod structure.

The incident photon-to-current conversion efficiency (IPCE) was investigated in 1.0 M NaOH electrolyte (pH = 14) at zero potential vs Ag/AgCl (1 V vs RHE). As shown in Figure 2b, an IPCE up to ~62% between 600–800 nm was measured for the GaAs/TiO_2/Ni core-shell nanorod photoanode, which is higher than the value reached by the GaAs/TiO_2 nanofilm photoanode (~38% between 600–800 nm) and GaAs/TiO_2/Ni top nanorods (~52%). As such, the IPCE measurements are in good agreement with the *J–V* measurements. The fluctuation of the IPCE spectral shape may be due to optical interference and scattering from the surface of non-active layers and nanostructures, which has previously been observed in photoelectrode coated with surface protection film and nanocatalyst.[16]

The stability of current density versus time (*J--t*) of all three GaAs photoanodes were investigated for three h in 1.0 M NaOH electrolyte (pH = 14) at 0 V vs Ag/AgCl (1.0 V vs RHE). As shown in Figure 2c, the photocurrent of the GaAs/TiO_2 nanofilm and GaAs/TiO_2/Ni top nanorod photoanodes decreased rapidly, which was attributed to significant photocorrosion. On the other hand, the GaAs photoanode protected by TiO_2/Ni core-shell nanorods, shows that a relatively high photocurrent can been sustained over this period. Although the photocurrents of the GaAs/TiO_2 nanofilm and GaAs/TiO_2/Ni top nanorods, and GaAs/TiO_2/Ni core-shell nanorods were degraded to about 4.10, 4.4 and 10.6 mA cm^{-2} after 1 h of operation, respectively (i.e., a 62, 56 and 15.6% loss in performance respectively), it was clear that the use of a 3D TiO_2/Ni hole-extraction layer can significantly enhance the stability of GaAs photoanodes. As both samples have the same thickness of the TiO_2 nanofilm, such an improvement is attributed to the efficient transfer of holes to the photoanode surfaces to oxidize water, and the avoidance of parasitic self-oxidation reactions by surface accumulated holes.

Time-resolved charge carrier behaviour

To obtain more insight regarding the charge transfer performance at the semiconductor/electrolyte interface, electrochemical impedance spectra (EIS) measurements were conducted using a standard three-electrode configuration in 1.0 M NaOH electrolyte (pH = 14) under dark conditions. The EIS measurements were obtained in the range of from 10 kHz to 3 MHz at an amplitude of 10 mV. The obtained data were fitted using the simple Randles equivalent circuit, shown in Figure 2d, with only one charge transfer resistance element (d) indicating a good ohmic contact between the GaAs photoanodes and the hosting substrate. As shown in Figure 2d, the GaAs/TiO_2/Ni core-shell nanorod photoanode shows a lower charge transfer resistance and higher conductivity compared to a GaAs/TiO_2 nanofilm and GaAs/TiO_2/Ni top nanorods photoanode, which confirms the improved carrier kinetics when using the 3D-TiO_2/Ni nanostructures.

The charge carrier behaviour was further investigated using transient absorption spectroscopy (TAS). This technique has previously been used to measure the charge carrier dynamics of a wide range of photoanode materials for water splitting; including α-Fe_2O_3,[19] $BiVO_4$,[20] WO_3[21] and TiO_2.[22] It has also been used to measure charge carrier separation and lifetime in heterojunction systems.[23]

Un-coated GaAs, GaAs/TiO_2 nanofilm and GaAs/TiO_2/Ni core-shell nanorods were studied in an argon atmosphere (in the absence of electrolyte, where photochemical reactions cannot occur).

This allowed us to measure intrinsic charge carrier relaxation kinetics.[24] The transient absorption decay dynamics (Figure S9) and spectra (Figure S10) of un-coated GaAs, GaAs/TiO_2 nanofilm and GaAs/TiO_2/Ni core-shell nanorods are provided in the Supporting Information. These transient decay dynamics (Figure S11) and spectra (Figure S12) are compared at select probe wavelengths and times, respectively. In un-coated GaAs, a broad bleach (i.e., a negative absorption) from ~900 to 1150 nm was observed at early timescales (10 μs), which recovered to form a positive signal by 100 μs. Similar early timescale bleaching was previously observed in α-Fe_2O_3 photoanodes, and was attributed to electron trapping by localized states located close to the conduction band edge, which results in a loss in the ground state absorption.[25] From 100 μs, a broad, positive absorption signal was observed in un-coated GaAs. These states were relatively long-lived and decayed to half the maximum ($t_{50\%}$) within ~0.2 s. Similar bleaching and recovery behaviour was observed in the GaAs/TiO_2 nanofilm; however, the recovery produced a significantly higher transient absorption signal (Figure 3a). This higher degree of absorption (~3 times higher than un-coated GaAs) is due to the presence of a higher population of charge carriers, and it was therefore clear that the formation of a GaAs/TiO_2 heterojunction inhibited early timescale recombination of photogenerated charge. Similar transient absorption signals were observed in GaAs/

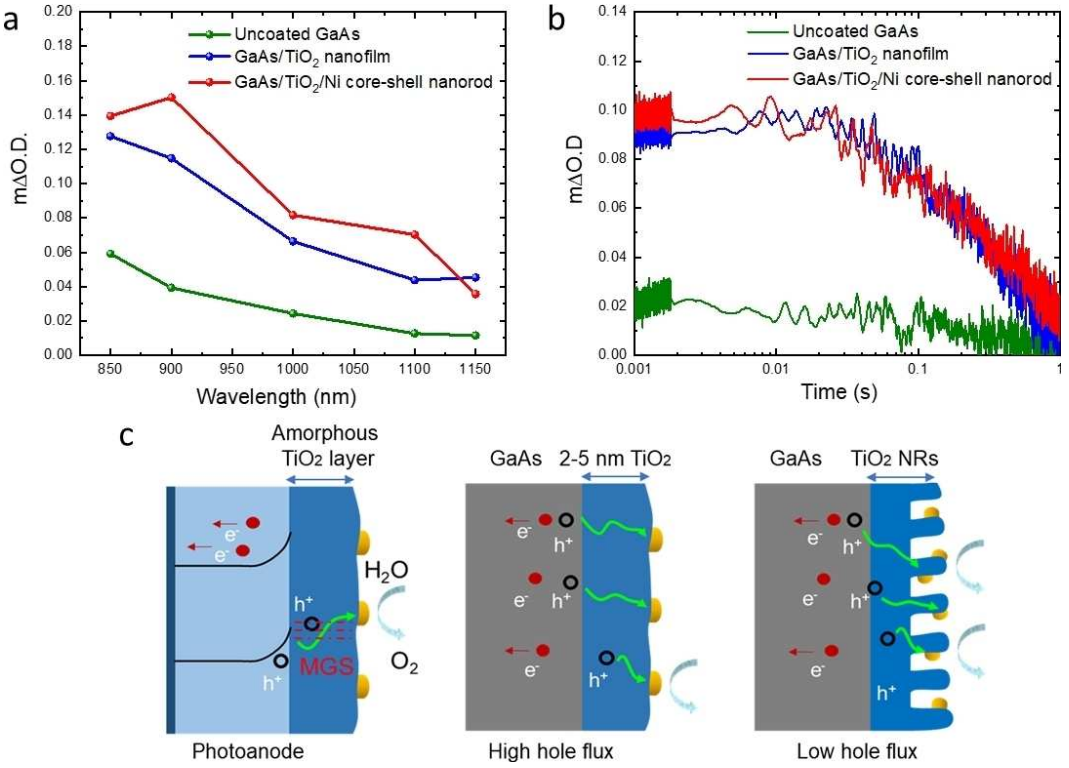

Figure 3. Transient absorption spectroscopy of GaAs, GaAs/TiO_2 nanofilm and GaAs/TiO_2/Ni core-shell nanorod. (a) Transient spectra at 10 ms after a laser pulse and (b) the transient absorption decay dynamics from 1 ms after a laser pulse (λ_{exc} = 355 nm, ~1.0 mJ cm^{-2} $pulse^{-1}$, 6 ns pulse width, 0.65 Hz). (c) Schematic illustration of the charge transfer at the GaAs/TiO_2 nanofilm, GaAs/TiO_2/Ni top nanorod, and GaAs/TiO_2/Ni core-shell nanorod interfaces.

TiO_2/Ni core-shell nanorods, the only difference being the rate of signal recovery from the bleach being significantly faster in this multi-layered material. The intrinsic charge carrier recombination dynamics in both GaAs/TiO_2 nanofilm and GaAs/TiO_2/Ni core-shell nanorods were similarly long-lived ($t_{50\%} \approx 0.2$ s, Figure 3b). As illustrated in Figure 3c, hole transfer from GaAs to the leaky amorphous TiO_2 layer occurs through mid-gap states in the TiO_2 layer. The formation of TiO_2 nanorods not only lead to a higher density of mid-gap states but also reduce the effective hole flux to facilitate charge transfer. Moreover, due to the fast transfer of holes to the 3D TiO_2 layer, accumulation of holes at the GaAs/TiO_2 interface is reduced, which is in agreement with transient absorption spectroscopy (TAS).

Stability of the GaAs photoanodes

To compare the degree of photocorrosion of both types of photoelectrodes, the surface morphology of the GaAs photoanodes surface was studied by scanning electron microscopy (SEM). Figure 4a–c shows the SEM images of the surfaces of GaAs/TiO_2 nanofilm, GaAs/TiO_2/Ni top nanorods, and GaAs/TiO_2/Ni core-shell nanorods after 3 h of stability testing. Both photoanodes show different degrees of photocorrosion. Although no signs of damage was observed by SEM in the GaAs/TiO_2/Ni core-shell sample, the PEC activity was shown to decrease over time (Figure 2d), and we attribute this to either the dissolution of the Ni catalyst or pit-hole corrosion in GaAs due to the formation of micro-cracks in the TiO_2 passivation layer. The GaAs/TiO_2 nanofilm and GaAs/TiO_2/Ni top nanorods photoanodes have been significantly etched leaving large and deep holes on the surface which may be attributed to removal of TiO_2 protection layer from the surface. X-ray photoelectron spectroscopy (XPS) analysis of the GaAs photoanodes was performed to probe the surface chemistry before and after the stability tests (Figure 4d,e). The GaAs/TiO_2 nanofilm and GaAs/TiO_2/Ni top nanorod photoanodes showed a dramatic change to their surface composition after stability tests. Prior to PEC testing both photoanodes showed the Ti 2p spectra indicating Ti in the 4^+ oxidation state and the presence of the TiO_2

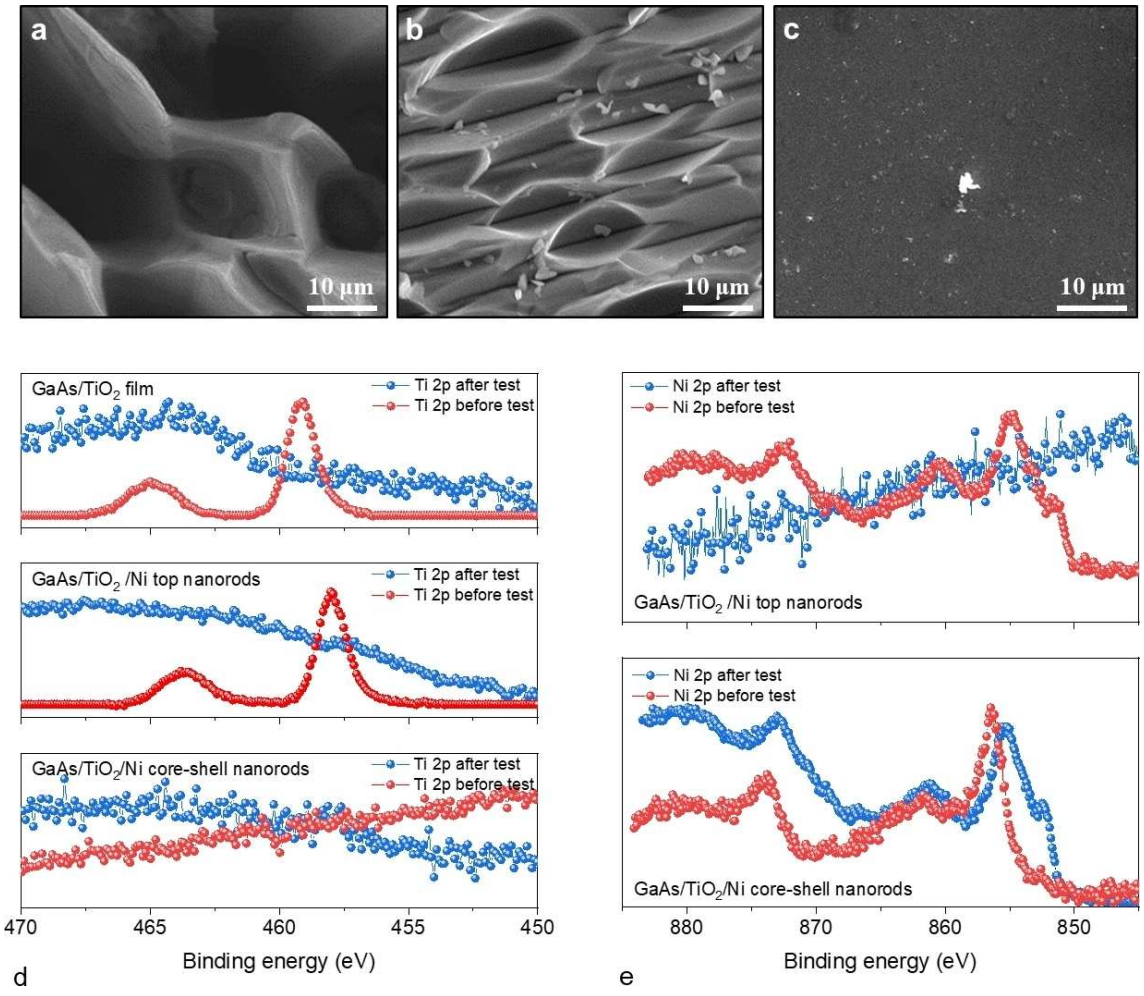

Figure 4. Reliability tests of both GaAs photoanodes before and after PEC testing for 3 h. SEM images of (a) GaAs/TiO_2 nanofilm photoanode, (b) GaAs/TiO_2/Ni top nanorod photoanode and (c) SEM image of GaAs/TiO_2/Ni core-shell nanorod photoanode after reliability test (3 h). XPS spectra showing the surface composition of the GaAs/TiO_2 nanofilm photoanode: (d) detailing the Ti 2p spectra of three photoanode samples before and after PEC measurement and (e) showing the Ni 2p spectra before and after PEC testing of the GaAs TiO_2/Ni top nanorod and GaAs/TiO_2/Ni core-shell nanorod photoanode samples.

protective layer.[26] For the GaAs/TiO_2/Ni top nanorod photoanode, NiO (native oxide) was also detected as evidenced by the Ni 2p spectrum. After PEC testing, both photoanodes showed a lack of TiO_2, as shown by the low levels of Ti 2p detected. Furthermore, for the GaAs/TiO_2/Ni top nanorod photoanode the Ni had also been completely degraded in the electrolyte. These XPS results for the nanofilm and nanorod photoanodes correspond well will the SEM images, in which the photoanodes were etched and damaged after PEC testing. Unlike these two photoanodes, the GaAs/TiO_2/Ni core-shell nanorods photoanode showed minimal change before and after PEC testing. XPS results for the Ni 2p region show that after PEC NiO (native oxide) was still present with some Ni metal being detected, presumably due to the native oxide being etched away in the electrolyte. No Ti was detected before and after PEC testing, providing further evidence for the integrity for the TiO/Ni core-shell structure, and corresponding well with SEM images.

Conclusions

Amorphous hierarchical TiO_2 nanostructures were deposited on the surface of GaAs photoanodes using glancing angle deposition. These 3D TiO_2 nanostructures not only serve as a surface protection layer but also an efficient hole-extraction layer that accelerates the oxygen evolution reaction and reduces photocorrosion. Upon the application of a Ni co-catalyst, the GaAs photoanodes showed an improvement in photocurrent and onset potential. More importantly, the growth of TiO_2 nanorods coverage by Ni catalyst resulted in a distinct improvement in the stability of the GaAs photoanode. These results pave the way for the realization of reliable GaAs-based photoanodes and significantly contribute to address their inherent stability issues.

Experimental Section

Fabrication of GaAs photoanodes

The wafer of (100)-oriented-GaAs was purchased from Wafer Technology LTD. The n-GaAs wafer was doped with Si and the thickness and carrier concentration are 625 μm and 1.6×10^{18} cm^{-3} respectively. The Ni/AuGe/Ni/Au (5 nm Ni/100 nm AuGe/35 nm Ni/300 nm Au) were deposited on the back side of a GaAs sample by thermal evaporation, to serve as a metal electrode for electron extraction in our photoanodes. The contact metals are alloyed at 400 °C for 30 s by rapid thermal annealing to form a good ohmic contact. Before the PEC experiments, the electrodes were attached by a copper wire using silver paste and covered by insulating epoxy.

GLAD deposition of TiO_2/Ni nanostructures

TiO_2/Ni nanostructures were grown on the surface of GaAs in a custom-built glancing angle deposition (GLAD) system with independent control over the substrate's azimuthal rotation ϕ, and the vapour flux angle α. All the depositions were performed at room temperature with a base pressure of 1×10^{-6} mbar.[27] Firstly, a conformal 5 nm thick TiO_2 layer was grown at $\alpha=0°$, without any azimuthal rotation (i.e., $\phi=0°$). Then, a 90 nm thick layer of TiO_2 was deposited at $\alpha=85°$, and the azimuthal rotation rates per unit thickness were $d\phi/d\theta=18\pm0.2°$ nm^{-1}, yielding ca. *xx* nm thick TiO_2 nanorods. Finally, 30 nm Ni was grown on the TiO_2 nanorods at $\alpha=45°$ or 87° while keeping $d\phi/d\theta=18\pm0.2°$ nm^{-1}, to respectively cover Ni only on top (Figure 1d) or the whole surface of the TiO_2 hybrid nanorods (Figure 1a).[28]

Materials characterisation

The high-resolution STEM (STEM) images were obtained using a Hitachi HD2700 STEM operated at 200 kV in high-angle annular dark field (HAADF) and bright filed modes. EDX data was acquired a Bruker Quantax system. The TEM sample was prepared by FEI FIB200 FIB and thinned to electron transparency. AFM images were acquired using a Veeco Dimension V Scanning Probe Microscope with tapping mode at atmospheric pressure with a Si cantilever with 10 nm of radius. SEM analysis was carried out using a Hitachi S-4800 SEM at 3 kV accelerating voltage. XPS measurements were performed with a Thermo monochromated aluminium k-alfa photoelectron spectrometer, using monochromic AlKα radiation (1486.7 eV). Survey scans were collected in the range of 0–1300 eV. High resolution peaks were used for the principal peaks of Ga, As, Ti and O, Ni, Au (spot size 400 μm). Data was analysed using CasaXPS software.

Photoelectrochemical measurements

A 200 W Xe arc lamp (66477-200HXF-R1 Mercury-Xenon) with an AM 1.5 G filter was used to produce simulated one sun illumination. The illumination intensity was calibrated using a silicon reference cell with a power meter (Thorlabs, Model PM100A). Before PEC experiments, the electrolyte was purged with Ar for 30 min. PEC measurements were performed in a three-electrode configuration using photoanodes as working electrode, Ag/AgCl as a reference electrode and platinum coil as the counter electrode in 1.0 M NaOH electrolyte (pH = 14) in a single compartment PEC cell with a quartz window. The measured potentials vs the Ag/AgCl were converted to the reversible hydrogen electrode (RHE) scale using the following Nernst equation:

$$E_{RHE} = E_{Ag/AgCl} + 0.059 \times pH + E^{0}_{Ag/AgCl}$$

Where $E_{Ag/AgCl}$ the potential is experimentally measured vs the Ag/AgCl (in saturated KCl) reference electrode, and $E_{Ag/AgCl}{}^{0}$ is the standard potential of Ag/AgCl at 25 °C (0.1976 V vs RHE). All linear sweep voltammetry measurements with a scan rate of 50 $mV\,s^{-1}$ were performed under both dark and illumination conditions using an Ivium CompactStat.

With use of a monochromator, the incident photon-to-current conversion efficiency (IPCE) was measured using the same three-electrode setup for PEC experiments, at 0 V vs Ag/AgCl (1 V vs RHE).

The IPCE was calculated using the equation:

$$IPCE = \frac{A \times J}{P_{mono} \times \lambda}$$

where $A = 1239.8$ V nm, J is the photocurrent density [mA cm^{-2}], P_{mono} is the monochromated illumination power intensity [mW cm^{-2}] and λ the wavelength [nm]. The photocurrent was obtained by subtracting the dark current from the light current.

Transient absorption spectroscopy

Transient absorption spectroscopy, from the microsecond to second timescale, was measured in the absence of electrolyte, in an inert gas (argon) environment. TAS experiments could not be performed in operando, as the materials were susceptible to photocorrosion. A Nd:YAG laser (OPOTEK Opolette 355 II, ~6 ns pulse width) was used as the excitation source, generating 355 nm UV light from the third harmonic. This UV light pulse was transmitted to the sample through a light guide. The laser power was ~1.0 mJ cm^{-2} $pulse^{-1}$ and was pulsed at a rate of 0.65 Hz. The probe light was a 100 W Bentham IL1 quartz halogen lamp. Long pass filters (Comar Instruments) were placed between the lamp and sample to minimize short wavelength irradiation of the sample. Transient changes in absorption/diffuse reflectance from the sample was collected by a 2″ diameter, 2″ focal length lens and relayed to a monochromator (Oriel Cornerstone 130) and measured at select wavelengths between 850 to 1150 nm. Time-resolved intensity data was collected with a Si photodiode (Hamamatsu S3071). Data at times faster than 3.6 ms was recorded by an oscilloscope (Tektronics DPO3012) after passing through an amplifier box (Costronics), whereas data slower than 3.6 ms was simultaneously recorded on a National Instrument DAQ card (NI USB-6251). Each kinetic trace was obtained from the average of between 100 and 500 laser pulses. Acquisitions were triggered by a photodiode (Thorlabs DET10 A) exposed to laser scatter. Data was acquired and processed using home-built software written in Labview.

Author contributions

M.A. and J.W. conceived the idea and wrote the manuscript. M.A. performed the PEC experiments. M.A., A.K., and M.G. analysed the data. I.P.P. and S.S. performed XPS and related analysis. J.W. and H.L. performed the growth of the samples. M.A. and J.W. carried out the STEM experiment for the for the sample and analysed the STEM and EDX mapping. F.C. performed SEM and AFM. A.K. carried out TAS measurements and their analysis. H.-H.J., T.C.L. and P.F. performed the GLAD deposition of Ti/Ni nanostructure. All authors reviewed and commented on the manuscript.

Acknowledgements

M.A. acknowledges support and funding from King Abdulaziz City for Science and Technology (KACST), Riyadh, Saudi Arabia A. K. thanks Imperial College London for a Junior Research Fellowship, the EPSRC for a Capital Award Emphasising Support for Early Career Researchers and the Royal Society for an Equipment Grant (RSG\R1\180434). M.A. would like to thank Dr. Dan Ren from Michael Grätzel's group for helpful discussions and comments about PEC measurements.

Keywords: GaAs · nanorods · photoanodes · transient-absorption spectroscopy · water splitting.

[1] R. C. Armstrong, C. Wolfram, K. P. de Jong, R. Gross, N. S. Lewis, B. Boardman, A. J. Ragauskas, K. Ehrhardt-Martinez, G. Crabtree, M. V. Ramana, *Nat. Energy* **2016**, *1*, 15020.
[2] a) M. G. Walter, E. L. Warren, J. R. McKone, S. W. Boettcher, Q. Mi, E. A. Santori, N. S. Lewis, *Chem. Rev.* **2010**, *110*, 6446–6473; b) O. Morton, *Nature* **2006**, *443*, 19–22.
[3] a) M. Grätzel, *Nature* **2001**, *414*, 338–344; b) J. A. Turner, *Science* **2004**, *305*, 972–974.
[4] a) J. Jian, Y. Shi, S. Ekeroth, J. Keraudy, M. Syväjärvi, R. Yakimova, U. Helmersson, J. Sun, *J. Mater. Chem. A* **2019**, *7*, 4721–4728; b) J. Luo, L. Steier, M. K. Son, M. Schreier, M. T. Mayer, M. Grätzel, *Nano Lett.* **2016**, *16*, 1848–1857; c) K. H. Ye, H. Li, D. Huang, S. Xiao, W. Qiu, M. Li, Y. Hu, W. Mai, H. Ji, S. Yang, *Nat. Commun.* **2019**, *10*, 3687.
[5] a) J. Wu, Y. Li, J. Kubota, K. Domen, M. Aagesen, T. Ward, A. Sanchez, R. Beanland, Y. Zhang, M. Tang, S. Hatch, A. Seeds, H. Liu, *Nano Lett.* **2014**, *14*, 2013–2018; b) M. Malizia, B. Seger, I. Chorkendorff, P. C. K. Vesborg, *J. Mater. Chem. A* **2014**, *2*, 6847–6853.
[6] a) M. Alqahtani, S. Sathasivam, A. Alhassan, F. Cui, S. BenJaber, C. Blackman, B. Zhang, Y. Qin, I. P. Parkin, S. Nakamura, H. Liu, J. Wu, *ACS Appl. Energy Mater.* **2018**, *1*, 6417–6424; b) M. Alqahtani, S. Sathasivam, L. Chen, P. Jurczak, R. Piron, C. Levallois, A. Létoublon, Y. Léger, S. Boyer-Richard, N. Bertru, J. M. Jancu, C. Cornet, J. Wu, I. P. Parkin, *Sustainable Energy Fuels* **2019**, *3*, 1720–1729.
[7] a) X. Lu, C. Zhao, *Nat. Commun.* **2015**, *6*, 6616; b) H. Inoue, T. Shimada, Y. Kou, Y. Nabetani, D. Masui, S. Takagi, H. Tachibana, *ChemSusChem* **2011**, *4*, 173–179; c) M. Alqahtani, S. Ben-Jabar, M. Ebaid, S. Sathasivam, P. Jurczak, X. Xia, A. Alromaeh, C. Blackman, Y. Qin, B. Zhang, B. S. Ooi, H. Liu, I. P. Parkin, J. Wu, *Opt. Express* **2019**, *27*, A364-A371.
[8] S. Oh, H. Song, J. Oh, *Nano Lett.* **2017**, *17*, 5416–5422.
[9] J. R. Bolton, S. J. Strickler, J. S. Connolly, *Nature* **1985**, *316*, 495–500.
[10] F. E. Osterloh, *Chem. Soc. Rev.* **2013**, *42*, 2294–2320.
[11] a) A. Fujishima, K. Honda, *Nature* **1972**, *238*, 37–38; b) K. Iwashina, A. Kudo, *J. Am. Chem. Soc.* **2011**, *133*, 13272–13275; c) M. Alqahtani, S. Sathasivam, F. Cui, L. Steier, X. Xia, C. Blackman, E. Kim, H. Shin, M. Benamara, Y. I. Mazur, G. J. Salamo, I. P. Parkin, H. Liu, J. Wu, *J. Mater. Chem.* **2019**.
[12] J. Zhao, T. M. Gill, X. Zheng, *Nano Res.* **2018**, *11*, 3499–3508.
[13] S. Hu, M. R. Shaner, J. A. Beardslee, M. Lichterman, B. S. Brunschwig, N. S. Lewis, *Science* **2014**, *344*, 1005–1009.
[14] a) A. G. Scheuermann, P. C. McIntyre, *J. Phys. Chem. Lett.* **2016**, *7*, 2867–2878; b) D. Bae, B. Seger, P. C. Vesborg, O. Hansen, I. Chorkendorff, *Chem. Soc. Rev.* **2017**, *46*, 1933–1954.
[15] a) A. Heller, H. J. Lewerenz, B. Miller, *Ber. Bunsenges. Phys. Chem.* **1980**, *84*, 592–595; b) P. Allongue, *J. Electrochem. Soc.* **1989**, *136*; c) K. W. Frese, Jr., M. J. Madou, S. R. Morrison, *J. Electrochem. Soc.* **1981**.
[16] Y. Su, C. Liu, S. Brittman, J. Tang, A. Fu, N. Kornienko, Q. Kong, P. Yang, *Nat. Nanotechnol.* **2016**, *11*, 609–612.
[17] M. V. Lebedev, W. Calvet, T. Mayer, W. Jaegermann, *J. Phys. Chem. C* **2014**, *118*, 12774–12781.
[18] S. Hu, M. H. Richter, M. F. Lichterman, J. Beardslee, T. Mayer, B. S. Brunschwig, N. S. Lewis, *J. Phys. Chem. C* **2016**, *120*, 3117–3129.
[19] F. Le Formal, S. R. Pendlebury, M. Cornuz, S. D. Tilley, M. Grätzel, J. R. Durrant, *J. Am. Chem. Soc.* **2014**, *136*, 2564–2574.
[20] Y. Ma, S. R. Pendlebury, A. Reynal, F. Le Formal, J. R. Durrant, *Chem. Sci.* **2014**, *5*, 2964–2973.
[21] S. Corby, L. Francas, S. Selim, M. Sachs, C. Blackman, A. Kafizas, J. R. Durrant, *J. Am. Chem. Soc.* **2018**, *140*, 16168–16177.
[22] A. Kafizas, Y. Ma, E. Pastor, S. R. Pendlebury, C. Mesa, L. Francàs, F. Le Formal, N. Noor, M. Ling, C. Sotelo-Vazquez, C. J. Carmalt, I. P. Parkin, J. R. Durrant, *ACS Catal.* **2017**, *7*, 4896–4903.
[23] a) A. Kafizas, X. Wang, S. R. Pendlebury, P. Barnes, M. Ling, C. Sotelo-Vazquez, R. Quesada-Cabrera, C. Li, I. P. Parkin, J. R. Durrant, *J. Phys. Chem. A* **2016**, *120*, 715–723; b) C. Sotelo-Vazquez, R. Quesada-Cabrera, M. Ling, D. O. Scanlon, A. Kafizas, P. K. Thakur, T.-L. Lee, A. Taylor, G. W.

Watson, R. G. Palgrave, J. R. Durrant, C. S. Blackman, I. P. Parkin, *Adv. Funct. Mater.* **2017**, *27*.
[24] X. Wang, A. Kafizas, X. Li, S. J. A. Moniz, P. J. T. Reardon, J. Tang, I. P. Parkin, J. R. Durrant, *J. Phys. Chem. C* **2015**, *119*, 10439–10447.
[25] S. R. Pendlebury, X. Wang, F. Le Formal, M. Cornuz, A. Kafizas, S. D. Tilley, M. Grätzel, J. R. Durrant, *J. Am. Chem. Soc.* **2014**, *136*, 9854–9857.
[26] M. C. Biesinger, L. W. M. Lau, A. R. Gerson, R. S. C. Smart, *Appl. Surf. Sci.* **2010**, *257*, 887–898.
[27] A. G. Mark, J. G. Gibbs, T. C. Lee, P. Fischer, *Nat. Mater.* **2013**, *12*, 802–807.
[28] H. H. Jeong, A. G. Mark, J. G. Gibbs, T. Reindl, U. Waizmann, J. Weis, P. Fischer, *Nanotechnology* **2014**, *25*, 235302.